Decoupling between Shockley partials and stacking faults strengthens multi-principal element alloys

Zongrui Pei^{a,1}, Siyuan Zhang^b, Yinkai Lei^c, Fan Zhang^d, and Mingwei Chen^e

^aOak Ridge National Laboratory, Oak Ridge, Tennessee 37831, USA; ^bMax-Planck-Institut für Eisenforschung GmbH, D-40237 Düsseldorf, Germany; ^cDepartment of Mechanical Engineering and Materials Science, University of Pittsburgh, Pennsylvania 15260, USA; ^dWPI Advanced Institute for Materials Research, Tohoku University, Sendai 980-8577, Japan; ^eDepartment of Materials Science and Engineering and Hopkins Extreme Materials Institute, Johns Hopkins University, Baltimore, Maryland 21218, USA

This manuscript was compiled on October 15, 2021

12

13

14

15

16

18

19

20

21

22

Mechanical properties are fundamental to structural materials, where dislocations play a decisive role in describing their mechanical behavior. Although the high yield stresses of multi-principal element alloys (MPEAs) have received extensive attention in the last decade, the relation between their mechanistic origins remains elusive. Our multi-scale study of density functional theory, atomistic simulations and high-resolution microscopy shows the excellent mechanical properties of MPEAs have diverse origins. The strengthening effects through Shockley partials and stacking faults can be decoupled in MPEAs, breaking the conventional wisdom that low stacking fault energies are coupled with wide partial dislocations. This study clarifies the mechanistic origins for the strengthening effects, laying the foundation for physics-informed predicative models for materials design.

 $\label{eq:multi-principal element alloys} \ | \ Strengthening \ mechanism \ | \ Stacking \\ fault \ energy \ | \ Dislocation$

ever-increasing interests from the physics and materials science community due to their huge unexplored compositional space and superior physical, mechanical and functional properties (1–12). They provide also an ideal platform to study fundamental physical mechanisms (9, 13–15). With the rise of MPEAs, understanding their mechanical properties has become a central topic in materials science in the last decade. In face-centered cubic (fcc) MPEAs, the motion of partial dislocations (Shockley partials) and their associated stacking faults (SF) defines their mechanical properties. Alloys with low stacking fault energies (SFEs) have more extended SFs, which are generally believed to have more strength and ductility through twinning-induced plasticity (TWIP) and transformation-induced plasticity (TRIP) mechanisms (16–18).

Although extensive endeavors have been made, the commonalities in the origins of high yield stresses shared by many MPEAs remain elusive. Among the most common intrinsic contributions of yield stresses are the lattice friction (or Peierls stress) and solute solution strengthening (19–23). Since the birth of MPEAs it has been a controversy about the relative importance of Peierls stress among the other contributions of yield stress, including the solid-solution strengthening effect (19, 22–24). Many researchers assume small Peierls stresses based on the common wisdom of conventional alloys and pure metals (25, 26) and the low SFEs in MPEAs. Low SFEs usually accompany small Peierls stresses. Overall, this controversy originates from the lack of accurate dislocation geometry in MPEAs, which allows for a direct, critical evaluation of the

Peierls stress. There are reports on the dislocation geometry in MPEAs, but almost all of them focused on the widths of SFs (27–29). In contrast, the core widths of Shockley partials are rarely reported for MPEAs, partly due to the difficulty in measurements and partly due to its importance has been unaware. To address this issue, we need very accurate determination of the core width of the Shockley partials. It is an important input parameter for mechanical simulations and various theories and models (22, 30–32). Here we adopt three of the most extensively studied MPEAs NiCoCr, VCoNi, CoCrFeNiMn and their only common fcc element Ni to address the above issues.

36

37

38

39

40

41

42

44

45

46

47

48

51

52

The commonalities in the origins of high yield stresses shared by the MPEAs can be indicated by the minimum energy profile along the dislocation motion path, i.e., the increased energies introduced by generalized stacking faults (GSFEs, see Fig. 1a). The local minima of the curves are SFEs and maxima are the theoretical energy barriers for pure shearing, which is a good indicator of the changes of Peierls stresses. Assisted by the accurate density functional theory (DFT), we compute GSFE curves for several representative MPEAs and their common fcc component Ni. This identifies a surprising fact: One of the representative MPEAs NiCoCr

Significance Statement

Alloys play crucial roles in the civilization history of human beings. Recently, a group of novel alloys without principal elements, i.e., multi-principal element alloys, have been extensively studied due to their excellent mechanical performance. Although we know many multi-principal element alloys have high yield stresses, the underlying mechanistic origins remain elusive. Assisted by state-of-the-art theoretical and experimental methods, we show the excellent mechanical properties have diverse origins. The strengthening effects through Shockley partials and stacking faults can change in different directions in these alloys, breaking the conventional wisdom. These new insights generalize the physical picture for the strengthening mechanisms that can coexist in the multi-principal element alloys and provide a new pathway to design high-performance alloys.

Z.P. conceived the ideas for the project; M.C. helped adjust the ideas; S.Z. analyzed the HAADF-STEM images that were taken by F.Z.; Y.L. did the MD simulations; Z.P. performed all the other calculations and wrote the manuscript; All authors participated in analysing the data and finalising the manuscript.

The authors declare no competing interests.

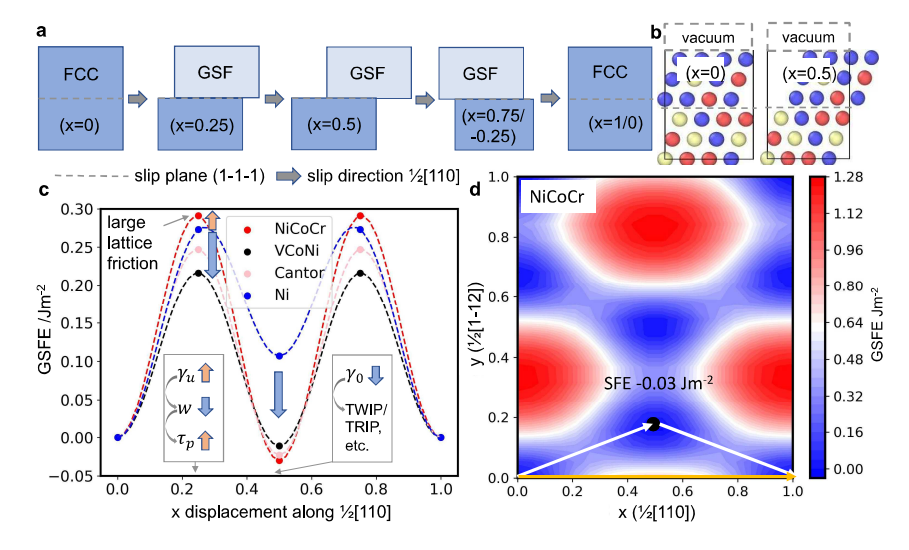


Fig. 1. GSFEs of three representative MPEAs and pure Ni. a, The schematic for the generation of GSFs along the slip direction. The displacement 0.75 is equivalent to -0.25 due to the adopted periodic boundary condition. b, The atom models at two representative displacements for GSFs. c, The dashed lines are the fitting of the data points to equation $\gamma = \gamma_0 \sin^2(\pi x) + (\gamma_u - \gamma_0/2) \sin^2(2\pi x)$ (34, 35). d, The GSFEs in c are along the path indicated by the white arrows on the gamma surface, i.e., the minimum energy projected along the path denoted by the orange arrow. The GSFE curves reveal the origin for the wide SF and smaller half width of Shockley partial of NiCoCr than Ni. We need to decrease SFE, while increases γ_u , in order to optimize the mechanical properties.

has a decoupled strengthening effects, i.e., it has narrower dislocation core of Shockley partial than pure Ni, although its SF is much wider than Ni. Usually in fcc alloys when SFE is lower its unstable SFE (maximal GSFE) is also lower, which is coupled. Examples include the two other MPEAs VCoNi and CoCrFeNiMn and many Mg alloys (basal plane dislocations) (26) and Al alloys (33). However, NiCoCr does not follow this convention. The understanding from multi-scale simulations, atomistic simulations and the high-angle annular dark-field scanning transmission electron microscopy (HAADF-STEM) images rationalizes the narrow core of Shockley partials. These results clearly reveal the diverse and decoupled mechanistic origins for the strengthening effects in the MPEAs with excellent mechanical properties.

Table 1. Comparison between the dislocation geometry of NiCoCr, VCoNi, CoCrFeNiMn and Ni. NiCoCr has a narrower core of Shockley partial than Ni, which is confirmed by DFT-informed Peierls-Nabarro model (DFT+PN) and EAM simulations.

| | $DFT + PN^a \; (DFT + PN^b)$ | EAM |
|-------------------------------|------------------------------|------|
| w(Ni)/w(NiCoCr) | 1.25 (1.16) | 1.15 |
| w(Ni)/w(VCoNi) | 0.88 (0.82) | - |
| $w({\sf Ni})/w({\sf Cantor})$ | 1.17 (1.05) | - |

^a DFT-computed SFEs for the three concentrated alloys; ^b Positive SFEs at room temperature for the alloys, e.g., $0.022~\mathrm{Jm}^{-2}$ for NiCoCr (37), $\sim 0.030~\mathrm{Jm}^{-2}$ for VCoNi (38) and $0.030~\mathrm{Jm}^{-2}$ for the Cantor alloy (27).

Decoupled mechanistic origins revealed by GSFEs

GSFE is a very useful tool to gain insight into the different mechanisms of deformation. For example, the unstable SFE (USFE, γ_u) indicates the contribution of Peierls stress; the magnitude of SFE offers information on the TRIP and TWIP deformation mechanism (17). Supercells of 72 atoms $(4(1/2[110]) \times 3(1/2[1\bar{1}2]) \times 6(1/3[1\bar{1}\bar{1}]))$ are employed to calculate GSFEs for Ni, VCoNi, NiCoCr and CoCrFeNiMn. Increasing the faulted planes from 6 to 12 only gives negligible changes of SFEs (-0.030 to -0.033 Jm⁻² for NiCoCr). Atoms are randomly placed on the lattice sites in the supercells for various configurations, and the number of configurations considered is determined by convergence tests (36) (e.g., Fig. S1). We calculate the GSFEs for three representative alloys with excellent mechanical properties and use their common for component Ni as a reference.

The GSFE curves of Ni, NiCoCr, VCoNi and CoCrFeNiMn (the Cantor alloy) are shown in Fig. 1 with key points listed in Table 1. It is worth mentioning that the curves in Fig. 1c are the GSFEs along the white arrows (1/6[112]) rather than the orange arrow (1/2[110]) in Fig. 1d. The common feature of all three alloys is that their lower SFEs help activate the various deformation modes facilitated by partial dislocations such as the TRIP mechanism. One surprising finding is that NiCoCr has a much lower SFE than Ni; its energy barrier USFE is however obviously higher than Ni. Given the relationship between SFE γ_0 and SF width $x_0 = \frac{\mu |\vec{b}|}{24\pi} \frac{b}{1-\nu} \frac{b^2 + \nu}{24\pi} \frac{1}{1-\nu}$

(Burgers vector \vec{b} , shear modulus μ and Poisson ratio ν), we find that Ni has a narrower SF width than NiCoCr. Here the SFE at room temperature for NiCoCr is adopted, e.g., 0.022 Jm⁻² (37). For a perfect dislocation when its restoring force takes a simple sinusoidal shape, its half width, i.e, the core width at the half height of its misfit-function peak, can be approximated by $w \approx Kb^2/4\pi\gamma_u$ (30). $K = \mu/(1-\nu)$ is an elastic constant for edge dislocation. This indicates the larger energy barrier of NiCoCr may give a smaller half width. However, this needs to be further confirmed by more accurate methods, since the formula for perfect dislocation may fail for dissociated dislocations.

The GSFEs of NiCoCr indicate the exceptional decoupling in the variation of dislocation geometry, i.e., SF widths and the half widths of Shockley partials can change in opposite directions, providing another pathway to tune mechanical properties. It is widely acknowledged that low SFE promotes the activation of the TWIP and TRIP mechanisms, making the alloy more ductile and stronger. The same origin applies to VCoNi and CoCrFeNiMn. In contrast to VCoNi and CoCrFeNiMn, NiCoCr is unique since its SFE is lower than pure Ni but the USFE is higher than Ni, demonstrating its excellent mechanical properties have an additional origin, i.e., the increased Peierls stress. The decoupled strengthening mechanisms in NiCoCr show the high yield stresses in MPEAs have diverse origins.

| material | SFE | USFE |
|----------|--|-----------------|
| Ni | 0.107,0.110(39),0.120-0.130(40) | 0.273,0.273(39) |
| NiCoCr | -0.030, -0.026(41),-0.024 (42) | 0.291 |
| VCoNi | -0.011 | 0.216 |
| Cantor | -0.023, -0.010~-0.050(43) | 0.247 |

Consequences of decoupled mechanisms confirmed by a revised Peierls-Nabarro model

122

123

124

125

126

127

128

130

131

132

133

134

135

136

138

139

140

145

146

147

148

149

152

153

154

155

157

159

160

161

162

163

164

165

166

167

168

169

170

We move forward to further check if the half width w of the Shockley partial in NiCoCr is indeed smaller than in pure Ni by modeling its geometry directly. This is one of the consequences of the increased USFE in NiCoCr. DFT is accurate to describe dislocation geometry (44, 45). However it is infeasible to describe MPEAs, given that MPEAs require a much larger supercell and longer relaxation time for each ionic step. Moreover, the random feature of MPEAs requires multiple calculations to sample over different atomic configurations for the same geometry, since only statistic geometry is practically meaningful. Specifically, NiCoCr is more stable in hexagonal close-packed (hcp) structure than in fcc at 0 K, which also makes direct DFT calculations of random alloys impractical. Fortunately, Peierls-Nabarro model and its many revised versions (26, 46–50) offer a more convenient method to inspect the dislocation geometry in Ni and NiCoCr.

One of the key input parameters for the revised Peierls-Nabarro model (50) is the gamma surface γ (see Fig. 1). The elastic constants and Burgers vectors for NiCoCr and CoCr-FeNiMn are adopted from the seminal paper of Varvenne et al. (22) We obtained these parameters from our DFT calculations for VCoNi, i.e., G = 77.7 GPa, b = 2.53Å; Poisson ratio ν is taken as 0.33 which is an average of their experimental values. The so-called multiple-equal-fractional-dislocation (MEFD) formulation (50) introduces one extra freedom to the original Peierls-Nabarro model, which is particularly useful for compact dislocation core. The calculated dislocation cores for NiCoCr and pure Ni are shown in Fig. 2. The SF width of NiCoCr is theoretically infinite, which is a direct consequence of its negative SFE. However, the SF width cannot be actually infinite in a literally finite size sample in experiment. They are demonstrated by very wide SFs profuse under high resolution microscopy. In contrast, the SF width of Ni is finite, which is about 5.5 times the Burgers vector. The half width of a Shockley partial in Ni is 0.70b, while that in NiCoCr is 0.56b, with a ratio of 1.25. At room temperature, negative SFEs can become positive (51-53), e.g., 0.022 Jm^{-2} for NiCoCr (37). Adoption of this room temperature SFE in our model yields only a slight change of half width from 0.56b to 0.62b, which is unambiguously smaller than 0.70b (0K) or 0.72b (room temperature) of pure Ni. This confirms the wider core of Ni than NiCoCr that is indicated by their USFEs γ_u . These results are listed in Table 1.

In addition to the GSFE method and DFT-informed Peierls-Nabarro modeling, we also adopt a modified embedded-atom method (MEAM) potential (54) to perform molecular statics calculations (55) for the same dislocations in NiCoCr and Ni. The displacement fields for the two systems are directly

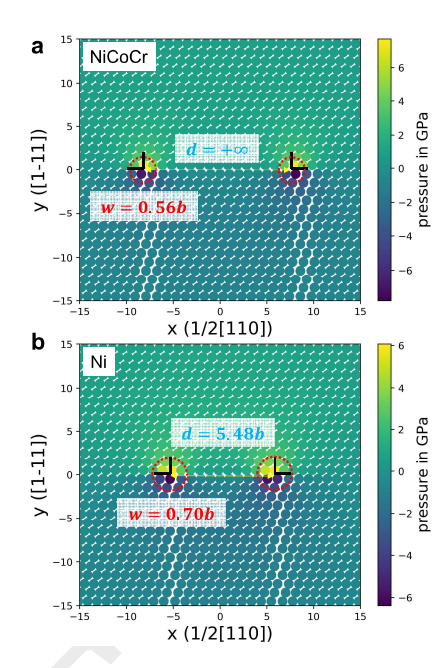


Fig. 2. The dislocation geometry of NiCoCr and Ni. The half widths for Shockley partials are featured. The dislocation core structures are calculated numerically by a revised Peierls-Nabarro model. Using SFEs at 0K in the model yields 0.56b for NiCoCr and 0.70b for pure Ni; when SFEs at room temperature are adopted for NiCoCr (37) and Ni (40), the half widths become 0.62b and 0.72b, respectively.

extracted from the relaxed atomistic structures and shown in Fig. S2. The displacement fields are then fitted to a Lorentzian peak $\rho(x;w)=w/(x^2+w^2)$, which yields the half width w for Shockley partials. The w of Ni is also wider than NiCoCr, with a ratio of $w(\mathrm{Ni})/w(\mathrm{NiCoCr}){=}1.15$. This is consistent with the above results.

171

172

173

174

175

176

177

179

180

181

182

183

184

185

186

187

188

189

190

191

192

194

195

196

197

198

199

200

201

Direct measurement of the half width of Shockley partials by HAADF-STEM

The half width of dislocation core is one of the key parameters that determine Peierls stress. Although the theoretical methods can reliably confirm the w in Ni is wider than that in NiCoCr (26), the accurate half width needs to be calculated from experimental measurements, since Peierls stress is sensitive to its magnitude (50). Some researchers measured dislocation geometry, but mainly the width of SFs (28, 29, 45). Few people measure the half width of Shockley partials in pure Ni, which is not easy because of the interference of its narrow SFs. Fortunately, the SFs of MPEAs are multiple times wider than Ni and the interference can be negligibly small. Here we will adopt the state-of-the-art processing techniques for HAADF-STEM images to accurately measure the core width of the Shockley partial in one representative MPEA, i.e., NiCoCr.

The profuse Shockley partials in deformed NiCoCr are taken by HAADF-STEM for a statistical analysis (Fig. 3a). We use several latest processing methods to extract the atomic positions from HAADF-STEM (57) (see Fig. 3). It treats each bright atomic position as a 2D distribution of the pixels (of the order of 100). The intensity is fitted to a 2D Gaussian function

of a bell shape, i.e.,
$$f(x,y) = A \exp\left(-\frac{(x-x_0)^2}{2a^2} - \frac{(y-y_0)^2}{2b^2}\right)$$
.
Here A is a prefactor, a, b are the variances along the two prin-

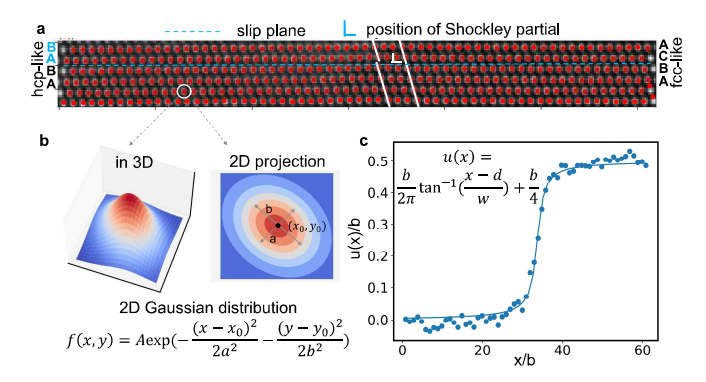


Fig. 3. Direct measurement of dislocation geometry by HAADF-STEM. $\bf a$, An example to show the extraction of atomic positions from HAADF-STEM using an accurate method implemented in Atomap (56). $\bf b$, The 2D Gaussian distribution used to fit the intensity distribution of the pixels around each atom in $\bf a$. The position (x_0,y_0) is adjusted according to its neighboring atoms. $\bf c$, The displacement field of the Shockley partial in $\bf a$ is fitted to an arc-tangent function to obtain the half width of Shockley partial.

cipal axes (see Fig. 3b). The mean (x_0, y_0) of the Gaussian function f(x,y) is considered as the position of that atom. Local distortion can be corrected or even removed by considering the nearest neighbors of the atom during the extraction process. This method is numerically accurate, repeatable and independent of researchers' experience. If the atoms are not in a line parallel to the horizontal direction but with an angle of θ , a correction of $1/\cos(\theta)$ is needed for the inter-atomic distances. The inter-atomic distances are rescaled by the average distance between atoms in the reference (defect-free) region. This can correct the inclination of the projection plane. See supplementary material for more details.

We analyze seven high-quality HAADF-STEM images with the above procedure to extract all relevant atomic positions. As is shown in Fig. 3c, we use arc-tangent function $u(x;w) = b/2\pi \arctan(x/w) + b/4$ to fit the HAADF-STEM atomic positions, which shows all the atomic positions approximately falling on the curve. The fitting yields a half width for NiCoCr with an average of $1.23b \pm 0.44b$. This is narrower than common pure metals with a range of $1.61b \sim 1.81b$ after considering a small correction factor (see supplementary material) (24, 58).

The fact that NiCoCr has a relative narrow core of Shockley partial is one of the important origins for its high yield stress. The small w can impact yield stress through both solid solution strengthening and Peierls stress. The former can be deduced from the Varvenne model (22). It predicts a higher yield stress for a narrow core of Shockley partials. The higher Peierls stress will be demonstrated in the following section.

Direct evaluation of Peierls stress

Peierls stresses can be calculated using an analytical formula (30) or the Peierls-Nabarro models, once the dislocation half width w is known. Peierls stress is very sensitive to the magnitude of half width, i.e., small variance in w results in substantial change of τ_p . The errors from the input parameters can be substantially mitigated by accurate techniques, such as accurate DFT calculations and reliable experimental measurements of dislocation core width.

In Fig. 4 we show the Peierls stresses calculated at various half width w by Peierls-Nabarro model with our MEFD

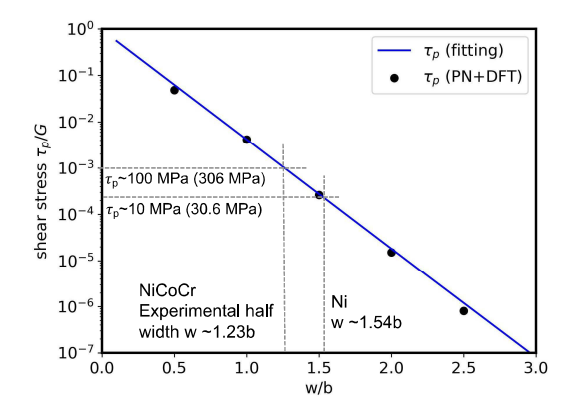


Fig. 4. Evaluations of the Peierls stresses for NiCoCr and Ni. The Peierls stress τ_p is determined jointly by experiment and revised Peierls-Nabarro model informed by DFT. The numbers in brackets are the contributions to yield stresses after a Taylor factor of 3.06 is included.

formulation. The analytical formula for Peierls stress of undissociated dislocations is $\tau_p/G = 1/(1-\nu) \exp(-2\pi w/b)$ (30), with a scaling factor of -2π between $\ln(\tau_p/G)$ and half width w/b. Obviously our DFT-informed method with a slope larger than -2π is less sensitive than the analytical formula. The Peierls stress at the experimental w for NiCoCr is denoted by dashed lines. As a reference, the Peierls stress of pure Ni at 1.54b (the DFT+PN ratio $1.25 \times 1.23b$ of NiCoCr measured by experiment) is also calculated. The Peierls stress, of the order of 100 MPa for NiCoCr, is much larger than common fcc metals such as Ni (of the order of several MPa) (25, 26), and cannot be ignored for quantitative accuracy. Its contribution to yield stress can be as large as several hundreds Megapascals. This numerically confirms one of the decoupled strengthening effects through lattice friction. Although this study focuses on edge dislocations that have lower resolved critical shear stress and thus dominate the yielding behavior, most of the conclusions hold for screw dislocations as well. The difference between edge and screw dislocation is a scaling factor in τ_p ."

In summary, we revealed the decoupled mechanistic origins for the excellent mechanical properties in the widely studied alloys. NiCoCr has a unique feature that its yield stress can be attributed to both its high lattice friction (narrow core of Shockley partials) and mechanisms through its low SFE; in contrast, the other representative alloys have smaller lattice friction than pure Ni, and their high yield stresses cannot be attributed to the lattice friction. This offers direct evidence for decoupled and diverse mechanistic origins for the strengthening effects in complex concentrated alloys. The decoupled strengthening mechanisms revealed here not only demonstrate the unusual flexibility of complex concentrated alloys to tune the mechanical properties but also provide a new pathway to design high-performance alloys.

Materials and Methods

Dislocation cores calculated from experiment. The Peierls stresses and dislocation cores of common pure metals were systematically studied by Kamimura *et al.* (58). The Peierls stresses of pure metals are usually of the order of 1-10 MPa, which are orders of

354 355 356 357

358

359

362

363

364

365

366

367

368

369

370

372

373

374

375

376

377

381

382

383

384

388

389

390

391

392

393

395

396

397

398

400

401

402

403

404

405

magnitude smaller than NiCoCr, which offers new insights into the deformation mechanisms of multi-principal element alloys

281

282

283

284

286 287

288

289

290

291

292

293

294

295

297

298

299

300

302

303

304

305

306

307

309

310

312

314

315

317

318

319

320

322

323

324

325

327

328

329

330

331

332

333

334

335

337

338

339

340

342

343

344

345

347

348

350

352

To correctly evaluate the half width of Shockley partials, several relations between the various quantities are needed. In Ref. (58), the values of h/b are tabulated, which is the distance between slip planes h divided by the magnitude of Burgers vector b. The half width can be obtained by $w/b=\frac{1}{1-v}h/b\approx 1.4h/b\approx 2.0$ when $h/b=1.41, \nu=0.3$. Therefore, for the metals (Cu, Ag, Au, Al, etc.), the half width w is about 2.0b. The reference does not include the value for Ni, which was calculated by Zhao and Nieh from experimental data (24). They showed pure Ni has a core structure of 1.77b comparable to the other metals but larger than 1.23b of NiCoCr after considering a small correction factor.

One note is needed here. These experimental half widths are for perfect dislocations, which is slightly different from that of Shockley partials. The difference is approximately controlled by the dislocation character factor $f = \sin^2(\theta)/(1-v) + \cos^2(\theta)$, where θ is the angle between Burgers vector and line direction. For Shockley partial $\theta = 60^{\circ}$; for perfect dislocation $\theta = 90^{\circ}$. This gives a ratio of w(perfect)/w(Shockley) = f(perfect)/f(Shockley) = 1.1 whenthe Poisson ratio takes 0.3. This is numerically confirmed by the well-known paper of Lu et al. (59), which gives a ratio of 1.16. After including this factor, we can still conclude that pure metals including Ni (1.61b - 1.81b) have larger half width than the 1.23b of NiCoCr.

Procedure to extract dislocation displacement field. Ingots of the equiatomic NiCoCr were produced by arc-melting from high-purity elemental metals (99.9 wt.%). The melted button was flipped and re-melted at least five times and then drop-casting into a rectangular cross-section mold with sizes of 19.4 mm×15.8 mm. The cast ingots were then sealed in an evacuated quartz tube and homogenized at 1473 K for 24 h. The ingots were subsequently cold rolled along the longitudinal ingot direction to sheets with a final thickness of The rolled sheets were then annealed at 1173 K for 1 h, followed by water cooling. The sheets were then deformed by shock loading (57). Atomic-resolution images of the NiCoCr samples were acquired by using the high-angle annular dark-field (HAADF) scanning transmission electron microscopy (STEM). Bright field STEM (BF-STEM) and HAADF-STEM images were acquired using a Gatan BF detector and an annular-type HAADF detector with the collection angles ranging from 100 to 267 mrad, which were performed using an aberration-corrected JEOLARM-200F transmission electron microscopy (TEM) operating at 200 kV. These images are firstly screened for high quality ones which clearly show the atomic positions in the dislocation core region. We then use Atoman (56) to extract the atomic coordinates for further processing to get the dislocation core. The atomic coordinates immediately above the slip plane $u_{+}(x)$ are subtracted from those below the slip plane $u_{-}(x)$ to get the displacement field $u(x) = u_{+}(x) - u_{-}(x)$; for those not parallel to the horizontal x direction and with a misorientation angle θ , a correction is made by $u(x)/\cos(\theta)$. The key techniques include (i) treating the each atom spot as a 2D Gaussian distributions with a elliptic shape, and taking the center of the ellipse as the atomic positions; (ii) adjusting the atom positions by considering the positions of neighboring atoms.

Density function theory calculations. Spin polarized density functional theory (DFT) (60, 61) simulations are carried out using Vienna Ab-initio Simulation Package (VASP) (62) to obtain the total energies for the generalized stacking fault energy (GSFE) calculations. The generalized gradient approximation (GGA) parametrized by Perdew-Burke-Ernzerhof (PBE) (63) is used to calculate the electronic exchange-correlation interaction, and the Kohn-Sham equation is solved using projector augmented wave (PAW) method (64), where the Brillouin zone is sampled using Monkhorst-Pack scheme (65). The atomic configurations of elements in the pseudo potentials used in our calculations are Co $[Ar]3d^84s^1$, Cr $[Ar]3d^54s^1$, Ni [Ar]3d⁸4s², Mn [Ar]3d⁶4s¹, Fe[Ar]3d⁷4s¹ and V [Ne3s²]3p⁶3d⁴4s¹. Supercells of 72 atoms are employed to calculate GSFEs for Ni, VCoNi, NiCoCr and CoCrFeNiMn. Once the lattice constants are optimized, only the ionic positions are relaxed in the GSFE calculations, the supercell shape and volume are fixed (ISIF=2). This is sufficient since we are interested in the trend of GSFE changes. The relaxation stops when the energy difference between ionic steps is

smaller than 10^{-4} eV. A plane wave cutoff of 350 eV and the k-point meshes of $6 \times 4 \times 4$ for Brillouin zone are used. An increase of k-point meshes by 8 times $(2 \times 2 \times 2)$, the change in total energy is less than 2 meV or 0.028 meV/atom. Multiple random configurations for the calculations of one GSFE, which allows us to evaluate the average and variance of the GSFE.

Revised Peierls-Nabarro modeling. The multiple-equal-fractionaldislocation (MEFD) formulation is used to solve the Peierls-Nabarro equation (50), where for dissociated edge dislocations, the edge and screw components of the trial misfit functions, $u_e(x)$ and $u_s(x)$, are

$$u_e(x) = \frac{b}{2\pi} \frac{1}{2N+1} \sum_{i=-N}^{N} \sum_{i=+1} \arctan\left(\frac{x - jd_0^e - id_1^e}{w_e}\right) + \frac{b}{2}, \quad [1a]$$

$$u_s(x) = \frac{\sqrt{3}b}{6\pi} \frac{1}{2N+1} \sum_{i=-N}^{N} \sum_{j=\pm 1}^{N} j \arctan\left(\frac{x - jd_0^s - id_1^s}{w_s}\right), \quad [1b]$$

where N is the number of arctangent functions for one partial, b is the magnitude of the Burgers vector for the perfect dislocation, wsignifies the half width of one Lorentzian peak. d_0 is the distance bewteen partials (50, 66). A total of six d, w parameters are optimized for each N using the Particle Swarm Optimization (PSO) algorithm (26, 66, 67). Here we adopt 100 particles and 100,000 steps for each optimization, which gives reliable results. The methods have been implemented in DIST (acronym for DIslocation Simulation Toolkit) toolkit (68). The MEFD formulation has been successfully used to study Mg (50), HEAs (20) and two-dimensional materials (69).

Dislocation cores by atomistic simulations. In addition to density functional theory, multi-scale modeling and experiment, atomistic simulations are also useful to indicate the relative magnitude of core widths of dislocations, although the quality of the results shall be carefully taken. The Large-scale Atomic/Molecular Massively Parallel Simulator (LAMMPS) (55) is used to optimize the core structure of the dislocations. Here we adopted one widely acknowledged modified embedded-atom method (MEAM) potential for such simulations (54). Periodic boundary condition is used in all three axes of the simulation cell. The conjugate gradient method is used to optimize both the atomic positions and the lengths of three cell axes at 0 K and the external pressure of 0 atm. The optimization stops when the force exerted on all atoms is less than 10^{-12} eV/Å. Our simulations use a supercell size of $100([110]) \times 5([\bar{1}12]) \times 10([1\bar{1}1])$. The perfect edge dislocation on the $[1\overline{1}1]$ plane is inserted at the center of the supercell. After relaxations, the atomic positions below and above the slip plane are extracted to calculate the displacement field for the dislocations. The displacement field is fitted to Lorentzian peaks to obtain the half width of Shockley partials. The procedure is similar to that for the experimental displacement field.

Supporting Information Appendix (SI). Supporting figures can be found in the supplementary material.

 $\label{eq:acknowledgments.} \textbf{ACKNOWLEDGMENTS.} \quad \text{This work was sponsored by the U.S.}$ Department of Energy, Office of Science, Basic Energy Sciences, Materials Science and Engineering Division. This research used resources of the Oak Ridge Leadership Computing Facility, which is supported by the Office of Science of the U.S. Department of Energy under Contract No. DE-AC05-00OR22725. M.C. acknowledges the support of U.S. National Science Foundation under grant DMR-1804320.

- 1. JW Yeh, et al., Nanostructured high-entropy alloys with multiple principal elements: Novel alloy design concepts and outcomes. Adv. Eng. Mater. 6, 299-303 (2004)
- 2. B Cantor, I Chang, P Knight, A Vincent, Microstructural development in equiatomic multicomponent alloys. Mater. Sci. Eng.: A 375-377, 213 - 218 (2004).

- Y Zhang, et al., Microstructures and properties of high-entropy alloys. *Progr. Mater. Sci.* 61,
 1 93 (2014).
- 4. EP George, D Raabe, RO Ritchie, High-entropy alloys. Nat. Rev. Mater. 4, 515-534 (2019).

409

410

415

416

417

418

425

426

433

434

444

445

457

458

459

460

- D Miracle, O Senkov, A critical review of high entropy alloys and related concepts. Acta Materialia 122, 448 – 511 (2017).
- R Zhang, et al., Short-range order and its impact on the CrCoNi medium-entropy alloy. *Nature* 581, 283–287 (2020).
- F Wang, et al., Multiplicity of dislocation pathways in a refractory multiprincipal element alloy.
 Science 370, 95–101 (2020).
 - S Wei, et al., Natural-mixing guided design of refractory high-entropy alloys with as-cast tensile ductility. Nat. Mater. 19, 1175–1181 (2020).
 - X Chen, et al., Direct observation of chemical short-range order in a medium-entropy alloy. Nature 592, 712–716 (2021).
- C Chen, et al., A novel ultrafine-grained high entropy alloy with excellent combination of mechanical and soft magnetic properties. J. Magn. Magn. Mater. 502, 166513 (2020).
- 420 intertrained and soft magnetic properties. *J. Magn. Magn. Mater.* 302, 166513 (2020).
 421 11. B Zhang, et al., Effects of cu and zn on microstructures and mechanical behavior of the medium-entropy aluminum alloy. *J. Alloy. Compd.* 820, 153092 (2020).
- medium-entropy aluminum alloy. J. Alloy. Compd. 820, 153092 (2020).
 J Joseph, et al., On the enhanced wear resistance of coorfemnni high entropy alloy at intermediate temperature. Scripta Materialia 186, 230–235 (2020).
 - R Zhang, et al., Short-range order and its impact on the crconi medium-entropy alloy. Nature 581, 283–287 (2020).
- I4. Z Pei, R Li, MC Gao, GM Stocks, Statistics of the nicoor medium-entropy alloy: Novel aspects
 of an old puzzle. npj Comput. Mater. 6, 1–6 (2020).
- the analysis of the state of th
- 16. B Gludovatz, et al., A fracture-resistant high-entropy alloy for cryogenic applications. Science
 345, 1153–1158 (2014).
 - Z Li, KG Pradeep, Y Deng, D Raabe, CC Tasan, Metastable high-entropy dual-phase alloys overcome the strength-ductility trade-off. Nature 534, 227–230 (2016).
- J Su, D Raabe, Z Li, Hierarchical microstructure design to tune the mechanical behavior of an interstitial TRIP-TWIP high-entropy alloy. Acta Materialia 163, 40–54 (2019).
- Z Wu, H Bei, G Pharr, E George, Temperature dependence of the mechanical properties of equiatomic solid solution alloys with face-centered cubic crystal structures. *Acta Materialia* 81, 428 – 441 (2014).
- X Liu, Z Pei, M Eisenbach, Dislocation core structures and peierls stresses of the high-entropy
 alloy nicofecrmn and its subsystems. *Mater. & Des.* 180, 107955 (2019).
- L Zhang, Y Xiang, J Han, DJ Srolovitz, The effect of randomness on the strength of highentropy alloys. Acta Materialia 166, 424–434 (2019).
 - C Varvenne, A Luque, WA Curtin, Theory of strengthening in fcc high entropy alloys. Acta Materialia 118, 164 – 176 (2016).
- SS Sohn, et al., Ultrastrong medium-entropy single-phase alloys designed via severe lattice distortion. Adv. Mater. 31, 1807142 (2019).
- distortion. Adv. Mater. 31, 1807142 (2019).
 Y Zhao, T Nieh, Correlation between lattice distortion and friction stress in ni-based equiatomic alloys. Intermetallics 86, 45–50 (2017).
- D Ma, M Friák, J von Pezold, J Neugebauer, D Raabe, Ab initio study of compositional trends in solid solution strengthening in metals with low peierls stresses. *Acta Materialia* 98, 367– 376 (2015).
- Z Pei, et al., From generalized stacking fault energies to dislocation properties: Five-energy
 point approach and solid solution effects in magnesium. *Phys. Rev. B* 92, 064107 (2015).
- NL Okamoto, et al., Size effect, critical resolved shear stress, stacking fault energy, and solid
 solution strengthening in the CrMnFeCoNi high-entropy alloy. Sci. reports 6, 35863 (2016).
 - TM Smith, et al., Atomic-scale characterization and modeling of 60 dislocations in a highentropy alloy. Acta Materialia 110, 352–363 (2016).
 - X Xu, et al., Transmission electron microscopy characterization of dislocation structure in a face-centered cubic high-entropy alloy Alo. 1CoCrFeNi. Acta Materialia 144, 107–115 (2018).
- B Joos, M Duesbery, The peierls stress of dislocations: an analytic formula. *Phys. Rev. Lett.* 78, 266 (1997).
- G Leibfried, HD Dietze, Versetzungsstrukturen in kubisch-flächenzentrierten kristallen. i.
 Zeitschrift für Physik 131, 113–129 (1951).
- Zeitschrift für Physik 131, 113–129 (1951).
 32. R Labusch, A statistical theory of solid solution hardening. physica status solidi (b) 41, 659–669 (1970).
- J Zhao, OM Løvvik, K Marthinsen, Y Li, Impurity effect of mg on the generalized planar fault energy of al. *J. materials science* 51, 6552–6568 (2016).
- Y Zeng, X Cai, M Koslowski, Effects of the stacking fault energy fluctuations on the strength ening of alloys. Acta Materialia 164, 1–11 (2019).
- 471 35. A Hunter, IJ Beyerlein, TC Germann, M Koslowski, Influence of the stacking fault energy
 472 surface on partial dislocations in fcc metals with a three-dimensional phase field dislocations
 473 dynamics model. *Phys. Rev. B* 84, 144108 (2011).
- 36. S Zhao, Y Osetsky, GM Stocks, Y Zhang, Local-environment dependence of stacking fault
 energies in concentrated solid-solution alloys. npj Comput. Mater. 5, 1–7 (2019).
- G Laplanche, et al., Reasons for the superior mechanical properties of medium-entropy cr coni compared to high-entropy crmnfeconi. *Acta Materialia* 128, 292–303 (2017).
- 38. DC Yang, YH Jo, Y Ikeda, F Körmann, SS Sohn, Effects of cryogenic temperature on tensile
 and impact properties in a medium-entropy vconi alloy. J. Mater. Sci. & Technol. 90, 159–167
 (2021).
- 39. DJ Siegel, Generalized stacking fault energies, ductilities, and twinnabilities of Ni and selected Ni alloys. Appl. Phys. Lett. 87, 121901 (2005).
- C Carter, S Holmes, The stacking-fault energy of nickel. The Philos. Mag. A J. Theor. Exp. Appl. Phys. 35, 1161–1172 (1977).
- H Huang, et al., Critical stress for twinning nucleation in crconi-based medium and high entropy alloys. Acta Materialia 149, 388–396 (2018).
 - Z Zhang, et al., Dislocation mechanisms and 3d twin architectures generate exceptional strength-ductility-toughness combination in crconi medium-entropy alloy. Nat. communications 8, 1–8 (2017).

 S Zhao, GM Stocks, Y Zhang, Stacking fault energies of face-centered cubic concentrated solid solution allovs. Acta Materialia 134, 334–345 (2017). 490

491

492

493

494

495

496

497

498

499

500

501

502

503

504

505

506

507

508

509

510

511

512

513

514

515

516

517

518

519

520

521

522

523

524

525

526

527

528

529

530

531

533

534

535

536

537

538

539

540

541

542

- L Ventelon, F Willaime, E Clouet, D Rodney, Ab initio investigation of the peierls potential of screw dislocations in bcc fe and w. Acta Materialia 61, 3973

 –3985 (2013).
- D Rodney, L Ventelon, E Clouet, L Pizzagalli, F Willaime, Ab initio modeling of dislocation core properties in metals and semiconductors. Acta Materialia 124, 633–659 (2017).
- VV Bulatov, E Kaxiras, Semidiscrete variational peierls framework for dislocation core properties. Phys. Rev. Lett. 78, 4221 (1997).
- 47. G Schoeck, The peierls model: progress and limitations. *Mater. Sci. Eng. A* **400**, 7–17 (2005).
- SF Wang, A unified dislocation equation from lattice statics. J. Phys. A: Math. Theor. 42, 025208 (2008).
- G Liu, X Cheng, J Wang, K Chen, Y Shen, Atomically informed nonlocal semi-discrete variational peierls-nabarro model for planar core dislocations. Sci. reports 7, 1–9 (2017).
- Z Pei, GM Stocks, Origin of the sensitivity in modeling the glide behaviour of dislocations. Int. J. Plast. 106. 48 – 56 (2018).
- S Huang, et al., Temperature dependent stacking fault energy of fecrconimn high entropy allov. Scripta Materialia 108, 44–47 (2015).
- J Ding, Q Yu, M Asta, RO Ritchie, Tunable stacking fault energies by tailoring local chemical order in crconi medium-entropy alloys. *Proc. Natl. Acad. Sci.* 115, 8919–8924 (2018).
- W Guo, et al., Shape-preserving machining produces gradient nanolaminate medium entropy alloys with high strain hardening capability. Acta Materialia 170, 176 – 186 (2019).
- WM Choi, YH Jo, SS Sohn, S Lee, BJ Lee, Understanding the physical metallurgy of the coorfemnni high-entropy alloy: an atomistic simulation study. npj Comput. Mater. 4, 1–9 (2018).
- S Plimpton, Fast parallel algorithms for short-range molecular dynamics. J. computational physics 117, 1–19 (1995).
- M Nord, PE Vullum, I MacLaren, T Tybell, R Holmestad, Atomap: a new software tool for the automated analysis of atomic resolution images using two-dimensional gaussian fitting. Adv. structural chemical imaging 3, 1–12 (2017).
- F Zhang, et al., Dislocation cooperation for hierarchical deformation in shock-loaded multiprincipal element alloys. submitted (2021).
- Y Kamimura, K Edagawa, S Takeuchi, Experimental evaluation of the peierls stresses in a variety of crystals and their relation to the crystal structure. Acta materialia 61, 294–309 (2013).
- G Lu, N Kioussis, VV Bulatov, E Kaxiras, Generalized-stacking-fault energy surface and dislocation properties of aluminum. *Phys. Rev. B* 62, 3099 (2000).
- 60. P Hohenberg, W Kohn. Phys. Rev. 136, B864 (1964).
- 61. W Kohn, LJ Sham. Phys. Rev 140, A1133 (1965).
- G Kresse, J Furthmüller, Efficient iterative schemes for ab initio total-energy calculations using a plane-wave basis set. *Phys. Rev. B* 54, 11169–11186 (1996).
- JP Perdew, K Burke, M Ernzerhof, Generalized gradient approximation made simple. Phys. Rev. Lett. 77, 3865–3868 (1996).
- 64. PE Blöchl, Projector augmented-wave method. Phys. Rev. B 50, 17953–17979 (1994).
- HJ Monkhorst, JD Pack, Special points for brillouin-zone integrations. *Phys. Rev. B* 13, 5188– 5192 (1976)
- Z Pei, An overview of modeling the stacking faults in lightweight and high-entropy alloys: Theory and application. *Mater. Sci. Eng. A* 737, 132 – 150 (2018).
- Z Pei, M Eisenbach, Acceleration of the particle swarm optimization for Peierls—Nabarro modeling of dislocations in conventional and high-entropy alloys. Comput. Phys. Commun. 215, 7 12 (2017).
- 68. Z Pei, Dist: A dislocation-simulation toolkit. Comput. Phys. Commun. 233, 44 50 (2018).
- Z Pei, S Mu, W Ming, The local strain distribution in bilayer materials: a multiscale study. Nanoscale 12, 6456–6461 (2020).

www.pnas.org/cgi/doi/10.1073/pnas.XXXXXXXXXX

487

488

489